*Strong Gravitational Lensing in the Era of Big Data*
*Proceedings IAU Symposium No. 381, 2024*
*H. Stacey, A. Sonnenfeld & C. Grillo, eds.*
doi:10.1017/S1743921323004131

# Angular structure and gravitational imaging

**Conor M. O'Riordan**

Max Planck Institut für Astrophysik, Karl-Schwarzschild-Straße 1, 85748 Garching bei München, Germany. email: conor@mpa-garching.mpg.de

**Abstract.** In gravitational imaging, the mass model for the main lensing galaxy is one of the main sources of systematic uncertainty. We use subhalo detection models with increasing levels of angular complexity in the lens mass model to analyse 100 HST mock observations. We find that perturbations of just 1% are enough to cause a 20% false positive subhalo detection rate, with order 3 multipoles having the strongest effect. The area in an observation where a substructure can be detected drops by a factor of 10 if multipoles up to 3 per cent amplitude are included in the lens model. The mass of the smallest detectable substructure however is not affected. We find a detection limit of $M > 10^{8.2} M_{\odot}$ at $5\sigma$ in all models. In order for strong lensing searches for dark matter objects to remain reliable in the future, angular structure beyond the elliptical power-law must be included.

**Keywords.** gravitational lensing, dark matter, machine learning

## 1. Introduction

Strong gravitational lensing has become one of the most important tools for investigating the nature of dark matter (Vegetti et al. 2023). This is because it can be used to detect dark matter subhaloes in the environments of galaxies. The existence of a large number of these subhaloes is a key prediction of the most popular dark matter model, cold dark matter (CDM) (Springel et al. 2008). With a technique called gravitational imaging, the number and mass of these subhaloes can be measured in strong lenses, constraining the underlying DM model (Vegetti and Koopmans 2009).

Gravitational imaging however is an expensive method. This is mostly due to the final stage of the analysis: so-called sensitivity mapping. Here, the observation is analysed to find the smallest detectable subhalo in each pixel (Despali et al. 2022). This information can be used to turn a set of subhalo detections and non-detections into an inference on the dark matter model. In O'Riordan et al. (2023) we introduced a machine learning technique that uses a set of large convolutional neural networks (CNNs) to replace the expensive sensitivity mapping stage. We exploited this new technique to test the sensitivity of *Euclid* strong lenses to dark matter subhaloes. Analysing 16,000 simulated *Euclid* strong lens observations we found that subhaloes with mass larger than $M = 10^{8.8 \pm 0.2} M_{\odot}$ could be detected at $3\sigma$ in that data, and that the entire survey should yield $\sim 2500$ new detections.

In the current work, we take our method much further to understand a crucial systematic uncertainty in subhalo detection: the angular complexity in the lens mass model. Strong lenses are typically modelled as elliptical power-laws, or some variation thereof. In this case the lens mass model has a strict elliptical symmetry, although it is often perturbed by an external shear component. We consider multipole perturbations to this simple model, where Fourier modes of order $m$ are added to the projected density of the

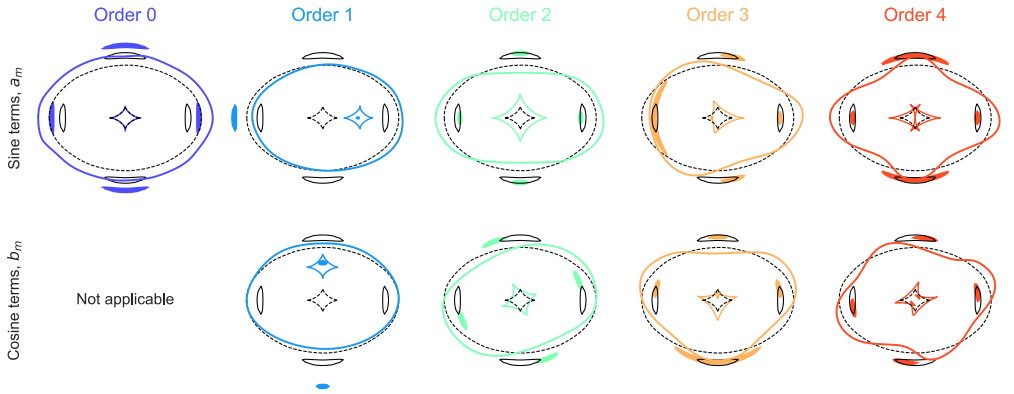


**Figure 1.** The effect on the critical curves, lensed images, and caustics from multipole perturbations. The macro model is an isothermal ellipsoid with axis ratio $q = 0.7$ and a source at the origin. The unperturbed critical curves and caustics are plotted as dashed black lines. The perturbed versions are plotted as solid coloured lines. In each case the perturbation is 0.1 in the respective coefficient.

galaxy. We use the definition given by Powell et al. (2022) for the convergence $\kappa_m$ due to a multipole of order $m$,

$$\kappa_m(\theta, \phi) = \theta^{1-\gamma} \left[a_m \sin(m\phi) + b_m \cos(m\phi)\right], \tag{1}$$

where $\theta$ is the angular radial distance from the centre of the lens, $\phi$ is the polar angle, $\gamma$ is the slope of the lensing galaxy power-law mass profile, and $a_m$ and $b_m$ are the sine and cosine amplitudes. For convenience we also define the multipole strength, $\eta_m$, and multipole angle, $\phi_m$, as

$$\eta_m^2 = a_m^2 + b_m^2, \tag{2}$$

$$\phi_m = \arctan(b_m/a_m), \tag{3}$$

respectively. Figure 1 shows the effect of these multipole perturbations on the lens. Perturbations of this nature are observed in the isophotes of elliptical galaxies (Bender and Moellenhoff 1987; Hao et al. 2006; Chaware et al. 2014; Mitsuda et al. 2017). Of particular importance is the $m = 4$ perturbation which gives rise to boxiness/disciness. This specific type of structure is motivated by the results of simulations, where it is expected to result from mergers (Naab et al. 1999).

The effect of these perturbations on measuring the Hubble constant in strong lenses has been studied by Van de Vyvere et al. (2022). The effect on substructure detection has not yet been systematically analysed, although multipole perturbations do feature in the lens models of some studies (e.g. Nightingale et al. 2022; Powell et al. 2022). Both of these examples find multipole amplitudes of order 0.01 in fits to real strong lenses.

We show that small changes in the angular structure of the lens galaxy can be easily mistaken for substructures when an insufficiently complex model is used. When a more complicated model is used, the area of the observation in which a substructure can be detected drastically changes, although the smallest detectable mass of substructure does not. We argue therefore that more angular complexity is required in strong lensing models for dark matter constraints to be reliable.

## 2. Method

We develop three neural networks to detect subhaloes in simulated strong lens images. The images have HST pixel scale and PSF. The source galaxies are taken directly from images of Hubble deep field (HDF) galaxies. Source galaxies are split into a training

https://doi.org/10.1017/S1743921323004131 Published online by Cambridge University Press

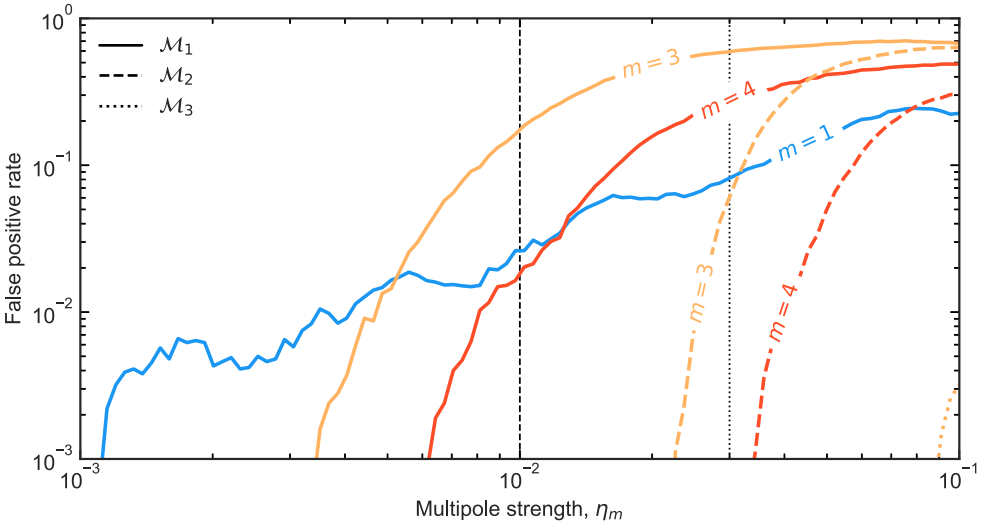


**Figure 2.** The rate of false positive substructure detection in observations with multipole perturbations but without subhaloes, as a function of multipole strength $\eta_m$ and order $m$. The multipole order used is labelled on each curve. The solid curves show the FPR for the model trained with no multipole perturbations.

and testing set. The testing set sources are also used for our results. Lens galaxies are elliptical power-laws. We place the lenses randomly in the volume of the HDF and look for sources in the light cone behind the lens. This produces realistic distributions of lens and source redshift, as well as Einstein radius. In producing training data we resample most lens and source parameters to produce as uniform a distribution of observations as possible. In our results, we use a set of 100 systems drawn from the realistic catalogue which resemble SLACS lenses Bolton et al. (2006). These have large, full Einstein rings with high S/N and are the lenses most useful for gravitational imaging.

To train the models we start with a parameter sweep to find the best initial learning rate. We optimise for the cross-entropy loss using the Adam optimiser. During training, when the loss on the testing data does not improve for 10 epochs, the learning rate is decayed by a factor $10^{-0.5}$. When three decays in learning have not improved the testing loss, the model is assumed to have converged. By the end of training, each model has seen $\sim 10^7$ unique strong lens images.

We label the three neural network models $\mathrm{M}_1$, $\mathrm{M}_2$ and $\mathrm{M}_3$. In $\mathrm{M}_1$, the training data only includes elliptical power-law lenses plus external shear up to a strength of $\gamma_{\mathrm{ext}} < 0.1$. In $\mathrm{M}_2$ and $\mathrm{M}_3$, random multipole perturbations of orders 1, 3, and 4 are present in the training data. The multipole strength is $\eta_m < 0.01$ in $\mathrm{M}_2$ and $\eta_m < 0.03$ in $\mathrm{M}_3$.

## 3. Results

Figure 2 shows the rate of false positive detections for the three trained models. At each multipole strength value we create 100 realisations of each of the 100 HST mock observations, with random multipole angles. These are passed through the detection models and the rate of $5\sigma$ detections is recorded. An amplitude of $\eta_m = 0.01$ causes a false positive subhalo detection 2.6 per cent, 18 per cent, and 2.0 per cent of the time for orders 1, 3, and 4 respectively. At $\eta_m = 0.03$ the same rates are 9.4 per cent, 61 per cent, and 30 per cent. At all multipole strengths, the order 3 perturbation is the most effective at causing false positive detections, with order 4 having a similar but weaker effect.

We use the three models to compute sensitivity maps for our 100 mock HST observations. The sensitivity maps give the lowest mass detectable subhalo in each pixel. Figure 3

https://doi.org/10.1017/S1743921323004131 Published online by Cambridge University Press

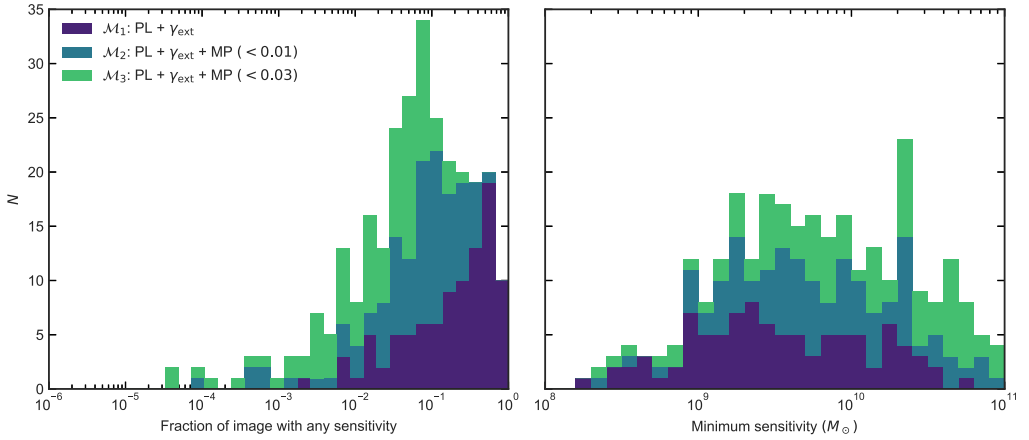


**Figure 3.** Summary statistics for sensitivity maps produced from our 100 mock HST observations, using all three models. Left: the fraction of the observation which is sensitive to any mass of substructure $M < 10^{11} M_\odot$ at $5\sigma$. Right: the detectable mass in the most sensitive pixel in each observation.

summarises the sensitivity maps in two statistics. On the left of the figure, we plot the total area in each observation which is sensitive to any mass using each model. When no multipoles are included in the model, 29 per cent of the area of all images is sensitive. This drops to 10 per cent when multipoles up to $\eta_m < 0.01$ are included and 3.6 per cent for $\eta_m < 0.03$. In contrast, the lowest detectable mass, plotted on the right of Fig. 3 does not change significantly between the three models. The most sensitive pixel in over all observations loses only 0.11 dex of sensitivity when including multipoles, with no further change when increasing the allowed size of the multipoles.

Sensitivity maps also allow one to calculate the expected number of detectable objects in an observation. A given dark matter model has a specific subhalo mass function, which is the number distribution of subhaloes on the sky as a function of mass. With the lowest detectable mass from the sensitivity map, we can integrate over this function to get the expected number of detectable objects in each pixel and sum over all pixels to get that number for each observation.

For the model with no included multipoles, and assuming CDM, we find 0.048 detectable objects per lens, or one detection in every $\sim 20$ observations. This is consistent with the frequency of detections in real HST data (Vegetti et al. 2014; Nightingale et al. 2022). When allowing for multipoles up to $\eta_m < 0.01$, this frequency drops to 0.0095 and 0.0047 for multipoles up to $\eta_m < 0.03$, equivalent to a detection once in every $\sim 100$ and $\sim 200$ lenses respectively.

## 4. Conclusions

When modelling gravitational lenses to reveal the presence of dark matter subhaloes, the lens mass model is a significant source of uncertainty. The angular complexity of the mass model is especially important, given that galaxies in nature can deviate significantly from the assumed elliptical symmetry of most analyses. In this work, we systematically analysed the degeneracy between non-elliptical angular structure in the lens galaxy, parameterised with multipole perturbations, and dark matter subhaloes. We found that small deviations from ellipticity, consistent with those found in nature, can cause a significant rate of false positive substructure detection when those deviations are not included in the lens model.

https://doi.org/10.1017/S1743921323004131 Published online by Cambridge University Press

Allowing for deviations from ellipticity in the lens model has a significant effect on the sensitivity of strong lens observations to dark matter substructure, reducing the area in the observation where a subhalo can be detected by up to a factor of 10. The minimum detectable subhalo mass however does not drastically change when including these perturbations. We therefore expect detections of subhaloes at the high-mass end, far from the lensed images to be most effected. These are also the least informative detections in terms of constraining dark matter models. We recommend therefore that future gravitational imaging efforts allow for complicated angular structure in the lens mass model, in order to remain reliable.

## References

Bender, R. & Moellenhoff, C. 1987, Morphological analysis of massive early-type galaxies in the Virgo Cluster. *A&A*, 177, 71–83.

Bolton, A. S., Burles, S., Koopmans, L. V. E., Treu, T., & Moustakas, L. A. 2006, The Sloan Lens ACS Survey. I. A Large Spectroscopically Selected Sample of Massive Early-Type Lens Galaxies. *ApJ*, 638(2), 703–724.

Chaware, L., Cannon, R., Kembhavi, A. K., Mahabal, A., & Pandey, S. K. 2014, Isophotal Shapes of Early-type Galaxies to Very Faint Levels. *ApJ*, 787(2), 102.

Despali, G., Vegetti, S., White, S. D. M., Powell, D. M., Stacey, H. R., Fassnacht, C. D., Rizzo, F., & Enzi, W. 2022, Detecting low-mass haloes with strong gravitational lensing I: the effect of data quality and lensing configuration. *MNRAS*, 510(2), 2480–2494.

Hao, C. N., Mao, S., Deng, Z. G., Xia, X. Y., & Wu, H. 2006, Isophotal shapes of elliptical/lenticular galaxies from the Sloan Digital Sky Survey. *MNRAS*, 370(3), 1339–1350.

Mitsuda, K., Doi, M., Morokuma, T., Suzuki, N., Yasuda, N., Perlmutter, S., Aldering, G., & Meyers, J. 2017, Isophote Shapes of Early-type Galaxies in Massive Clusters at z $\sim$ 1 and 0. *ApJ*, 834(2), 109.

Naab, T., Burkert, A., & Hernquist, L. 1999, On the Formation of Boxy and Disky Elliptical Galaxies. *ApJ*, 523(2), L133–L136.

Nightingale, J. W., He, Q., Cao, X., Amvrosiadis, A., Etherington, A., Frenk, C. S., Hayes, R. G., Robertson, A., Cole, S., Lange, S., Li, R., & Massey, R. 2022, Scanning For Dark Matter Subhalos in Hubble Space Telescope Imaging of 54 Strong Lenses. *arXiv e-prints*, arXiv:2209.10566.

O'Riordan, C. M., Despali, G., Vegetti, S., Lovell, M. R., & Moliné, Á. 2023, Sensitivity of strong lensing observations to dark matter substructure: a case study with Euclid. *MNRAS*, 521(2), 2342–2356.

Powell, D. M., Vegetti, S., McKean, J. P., Spingola, C., Stacey, H. R., & Fassnacht, C. D. 2022, A lensed radio jet at milliarcsecond resolution I: Bayesian comparison of parametric lens models. *MNRAS*, 516(2), 1808–1828.

Springel, V., Wang, J., Vogelsberger, M., Ludlow, A., Jenkins, A., Helmi, A., Navarro, J. F., Frenk, C. S., & White, S. D. M. 2008, The Aquarius Project: the subhaloes of galactic haloes. *MNRAS*, 391(4), 1685–1711.

Van de Vyvere, L., Gomer, M. R., Sluse, D., Xu, D., Birrer, S., Galan, A., & Vernardos, G. 2022, TDCOSMO. VII. Boxyness/discyness in lensing galaxies: Detectability and impact on $H_0$. *A&A*, 659, A127.

Vegetti, S., Birrer, S., Despali, G., Fassnacht, C. D., Gilman, D., Hezaveh, Y., Perreault Levasseur, L., McKean, J. P., Powell, D. M., O'Riordan, C. M., & Vernardos, G. 2023, Strong gravitational lensing as a probe of dark matter. *arXiv e-prints*, arXiv:2306.11781.

Vegetti, S. & Koopmans, L. V. E. 2009, Bayesian strong gravitational-lens modelling on adaptive grids: objective detection of mass substructure in Galaxies. *MNRAS*, 392(3), 945–963.

Vegetti, S., Koopmans, L. V. E., Auger, M. W., Treu, T., & Bolton, A. S. 2014, Inference of the cold dark matter substructure mass function at z = 0.2 using strong gravitational lenses. *MNRAS*, 442(3), 2017–2035.